Determining the Flight Icing Threat to Aircraft with Single-Layer Cloud Parameters Derived from Operational Satellite Data

WILLIAM L. SMITH JR. AND PATRICK MINNIS

NASA Langley Research Center, Hampton, Virginia

CECILIA FLEEGER, DOUGLAS SPANGENBERG, AND RABINDRA PALIKONDA

Science Systems and Applications, Inc., Hampton, Virginia

LOUIS NGUYEN

NASA Langley Research Center, Hampton, Virginia

(Manuscript received 21 February 2012, in final form 1 June 2012)

ABSTRACT

An algorithm is developed to determine the flight icing threat to aircraft utilizing quantitative information on clouds derived from meteorological satellite data as input. Algorithm inputs include the satellite-derived cloud-top temperature, thermodynamic phase, water path, and effective droplet size. The icing-top and -base altitude boundaries are estimated from the satellite-derived cloud-top and -base altitudes using the freezing level obtained from numerical weather analyses or a lapse-rate approach. The product is available at the nominal resolution of the satellite pixel. Aircraft pilot reports (PIREPs) over the United States and southern Canada provide direct observations of icing and are used extensively in the algorithm development and validation on the basis of correlations with Geostationary Operational Environmental Satellite imager data. Verification studies using PIREPs, Tropospheric Airborne Meteorological Data Reporting, and NASA Icing Remote Sensing System data indicate that the satellite algorithm performs reasonably well, particularly during the daytime. The algorithm is currently being run routinely using data taken from a variety of satellites across the globe and is providing useful information on icing conditions at high spatial and temporal resolutions that are unavailable from any other source.

1. Introduction

It is natural for clouds to contain supercooled liquid water (SLW) droplets at altitudes where the air temperature is below freezing. When SLW comes in contact with a hard surface such as the frame of an aircraft, it freezes, thereby icing the airframe. As ice accumulates on an aircraft, it alters the airflow, which can increase drag and reduce the ability of the airframe to create lift, leading to control problems with potentially disastrous consequences. Over the last half-century, a significant percentage of weather-related aviation accidents have been attributed to icing (National Aviation Safety Data Analysis Center 2005). Typically, the flight icing threat (FIT) to aircraft is reduced by avoidance or by protecting the aircraft with deicing and/or anti-icing equipment. Severe icing can overwhelm an aircraft's icing protection system, however. Model analyses, forecasts, and pilot reports (PIREPs) currently constitute much of the database available to pilots for assessing the icing conditions in a particular area. Such data may be uncertain or sparsely available. Icing conditions can be highly variable, often occurring in small areas that cannot be resolved with current icing diagnosis and forecasting methods, which tend to overestimate the areal coverage of the FIT. Thus, avoidance can be expensive, resulting in significant increases in flight time or delays on the ground. Although there have been improvements in systems to mitigate aircraft icing, no aspect of aircraft operations is immune to the threat.

The intensity of aircraft icing depends on meteorological factors, including the cloud temperature, liquid

Corresponding author address: William L. Smith Jr., NASA Langley Research Center, MS 420, Hampton, VA 23681.
E-mail: william.l.smith@nasa.gov

DOI: 10.1175/JAMC-D-12-057.1

© 2012 American Meteorological Society

water content, and droplet size (Rasmussen et al. 1992), and the level of severity depends on the intensity as well as on characteristics of the airframe and flight parameters. Because it is possible to infer these meteorological factors, or closely related cloud parameters, from satellite data (Minnis et al. 1995, 2004, 2011a), and because SLW is often found to reside in the top several hundred meters of cloud layers (Rauber and Tokay 1991), satellite data can be used advantageously to diagnose icing conditions. Curry and Liu (1992) developed an icing product that is based on cloud parameters derived for SLW clouds using microwave satellite remote sensing data. This technique is limited to the data with relatively low spatial and temporal resolution taken over oceanic regions from spaceborne meteorological microwave sensors, and this is perhaps most relevant for military applications. Ellrod and Nelson (1996) developed a multispectral thresholding technique using Geostationary Operational Environmental Satellite (GOES) imager data to discriminate clouds likely to be composed of SLW at cloud top. That product was later enhanced with estimates of cloud-top altitude to provide an upper altitude boundary for the icing layer (Ellrod and Bailey 2007), but no information on the base altitude or icing intensity was determined. Thompson et al. (1997) used satellite data to improve icing diagnoses on the basis of numerical weather analyses by eliminating areas with warm cloud tops.

Bernstein et al. (2005) describe methods to identify and forecast areas with potential aircraft icing conditions by blending relevant data from multiple sources such as satellite, surface, radar, lightning, and routine PIREPs with model forecasts of temperature, relative humidity, SLW, and vertical velocity. The current and forecast icing products (CIP and FIP, respectively) resulting from this comprehensive approach are proving useful to the aviation community and are available over the contiguous United States (CONUS) and southern Canada in near–real time as supplementary information at the National Oceanic and Atmospheric Administration (NOAA) Aviation Weather Center. Although research is under way for incorporating satellite-derived cloud properties in the CIP (Haggerty et al. 2008), the current version only uses satellite data in a rudimentary way as in Thompson et al. (1997). Smith et al. (2000) employed a theoretically based cloud parameter retrieval system to identify SLW clouds and found excellent correspondence with icing PIREPs provided that high-level ice clouds did not obscure the satellite field of view. Smith et al. (2003) found reasonably good correspondence between the cloud liquid water path (LWP) and effective radius R_e derived for SLW clouds from *GOES-8* data and similar parameters derived from surface-based remote sensors and aircraft in situ measurements. They also found a weak correlation between the LWP and PIREP icing intensity. Minnis et al. (2004) exploited these relationships and developed a satellite-based icing algorithm that is based on satellite-derived cloud parameters. Bernstein et al. (2006) found that it was particularly useful for directing a research aircraft into icing conditions. That algorithm was selected as the prototype candidate algorithm for the NOAA GOES-R program. NOAA is developing a suite of algorithms to derive geophysical parameters from its next-generation geostationary satellite system to improve weather forecasting and diagnoses of hazardous weather. Under sponsorship by the GOES-R Algorithm Working Group, an advanced version of the algorithm has been developed, demonstrated, tested, and delivered to the GOES-R program office.

The purpose of this paper is to describe the first-generation FIT algorithm developed for GOES-R and efforts to validate and demonstrate the potential utility to the aviation community using current GOES data. The theoretical basis for the algorithm is discussed, and the current formulation is described. The satellite-based icing diagnoses are compared with icing PIREPs, Tropospheric Airborne Meteorological Data Reporting (TAMDAR), and National Aeronautics and Space Administration (NASA) Icing Remote Sensing System (NIRSS) data. The paper concludes with a summary of the validation work and expectations for future improvements. Note that the algorithm and nomenclature presented here refer to the icing hazard associated with naturally occurring SLW in the atmosphere. A more mysterious icing hazard known to cause jet engine power loss and damage as a result of cloud ice particle ingestion (e.g., Mason et al. 2006) is a different phenomenon that is being addressed elsewhere and in future studies.

2. Data

Although aircraft icing conditions can form anywhere, they are most commonly found in two geographical regions over North America (Bernstein et al. 2007). The first includes the Pacific Northwest, western British Columbia in Canada, and Alaska. The second extends from the Canadian Maritimes stretching west and southwest to encompass the Great Lakes region, Ohio River Valley, and Hudson Bay. Much of this area is within the observation domain of the GOES imagers (*GOES-W* and *GOES-E*), which are well suited to monitor the evolution of clouds and associated weather conditions because of their relatively high spatial and temporal resolutions, nominally 4 km (1 km) in the

infrared (visible), and every 15 min. There fortunately are a number of other observing systems in this domain that characterize icing conditions that can be used to develop, demonstrate, and corroborate the satellite-based FIT. Icing PIREPs, TAMDAR, and NIRSS, respectively, offer direct subjective, direct objective, and ground-based remote observations of icing conditions. These data and their associated products are described in more detail below.

a. GOES-derived cloud products

For over a decade, NASA Langley Research Center (LaRC) has been routinely deriving cloud parameters from GOES imager data and has made these products available to the scientific and weather forecasting communities (Minnis et al. 2008a). The cloud retrieval methods were developed for application to the Moderate Resolution Imaging Spectroradiometer (MODIS) for the Clouds and the Earth's Radiant Energy System (CERES) global climate program (Minnis et al. 2011a) and have been adapted for application to GOES data beginning with *GOES-8* in the late 1990s. The primary algorithms used to derive cloud properties from GOES radiance data are the visible–infrared–solar-infrared–split-window technique (VISST) and solar-infrared–infrared–split-window technique (SIST). The VISST operates during the daytime using the 0.65-, 3.9-, 11-, and 12- (or 13.3) μm channels, whereas the SIST operates at night using the 3.9-, 11-, and 12- (or 13.3) μm channels. Cloudy pixels are determined using the method described by Minnis et al. (2008b). Cloud parameters are derived for the cloudy pixels using a set of parameterizations of the Earth–atmosphere solar reflectance (during daytime) and infrared emittance (day and night) models that incorporate cloud contributions for each relevant wavelength to match the observed satellite radiances with radiative transfer calculations using the assumption that each cloud layer is composed of either ice crystals or water droplets (Minnis et al. 2011a). In the real-time processing system, the GOES imager data are sampled from 4 km to 8 km to reduce the latency in producing the cloud products that is due to limited computational resources. In addition to LWP and R_e, the GOES-derived cloud products (GDCP) include the cloud phase, effective ice particle diameter D_e, ice water path (IWP), optical depth (COD), effective temperature T_c, height Z_c, and pressure P_c; cloud thickness ΔZ; and cloud-top height Z_t and pressure P_t. The cloud optical properties can be derived for a wide range of cloud thicknesses during the daytime since the solar reflectance at visible wavelengths is sensitive to changes in COD from values of less than 1 to values over 100. Since only infrared channels are available from GOES at night, there is little sensitivity to variations in COD for optically thick clouds. Thus, at night, cloud optical properties are only derived for optically thin clouds (COD < 6).

The LaRC CERES and GOES cloud products have been rigorously validated with cloud parameters derived from ground-based remote sensing and in situ data collected at the U.S. Department of Energy (DOE) Atmospheric Radiation Measurement (ARM) Program sites (Dong et al. 2002, 2008; Smith et al. 2008, Xi et al. 2010, and others). They have also recently been favorably compared to cloud parameters derived from active remote sensors aboard the *Ice, Cloud, and Land Elevation Satellite* (*ICESat*), the *Cloud–Aerosol Lidar and Infrared Pathfinder Satellite Observations* (*CALIPSO*) and *CloudSat* satellites (e.g., Minnis et al. 2008c, 2011b). An example of the LaRC cloud products derived from *GOES-10* and *GOES-12* is shown in Fig. 1, which depicts the retrieved cloud-top phase, Z_t, COD, R_e, LWP, and the cloud-base altitude Z_b, which is from the difference between Z_t and ΔZ. These parameters provide unique information about clouds that can be used to infer the potential for aircraft icing. For example, the cloud-top temperature (not shown) and cloud-top phase can be used to detect the presence of SLW. In this example, a large area of SLW (denoted by the cyan color in Fig. 1a) is detected over much of the upper Midwest and southern Canada in association with a storm system centered over the Great Lakes. The associated SLW droplet sizes and their densities can be inferred from the R_e and LWP images in Figs. 1d and 1e while Z_t and Z_b, shown in Figs. 1b and 1f, respectively, provide upper and lower altitude boundaries for the potential icing layers. These satellite-derived parameters are critical inputs to the FIT algorithm described below.

b. Icing PIREPs

PIREPs constitute the most widely available direct observations of in-flight icing conditions, particularly over the CONUS, and thus are used extensively in algorithm development and validation despite the fact that they have known deficiencies (Kane et al. 1998). They are spatially and temporally biased, and the biases are not systematic. Many years of experience with icing research aircraft, from which icing PIREPs were routinely filed, indicate that geolocation errors are on the order of 10–20 km [F. McDonough, University Corporation for Atmospheric Research (UCAR), 2010, personal communication]. PIREPs include intensity reports, which should be useful for validating the satellite algorithm. The intensity reports are subjective, however, and are based on pilot experience as well as on airframe and flight characteristics, and thus they can be difficult to

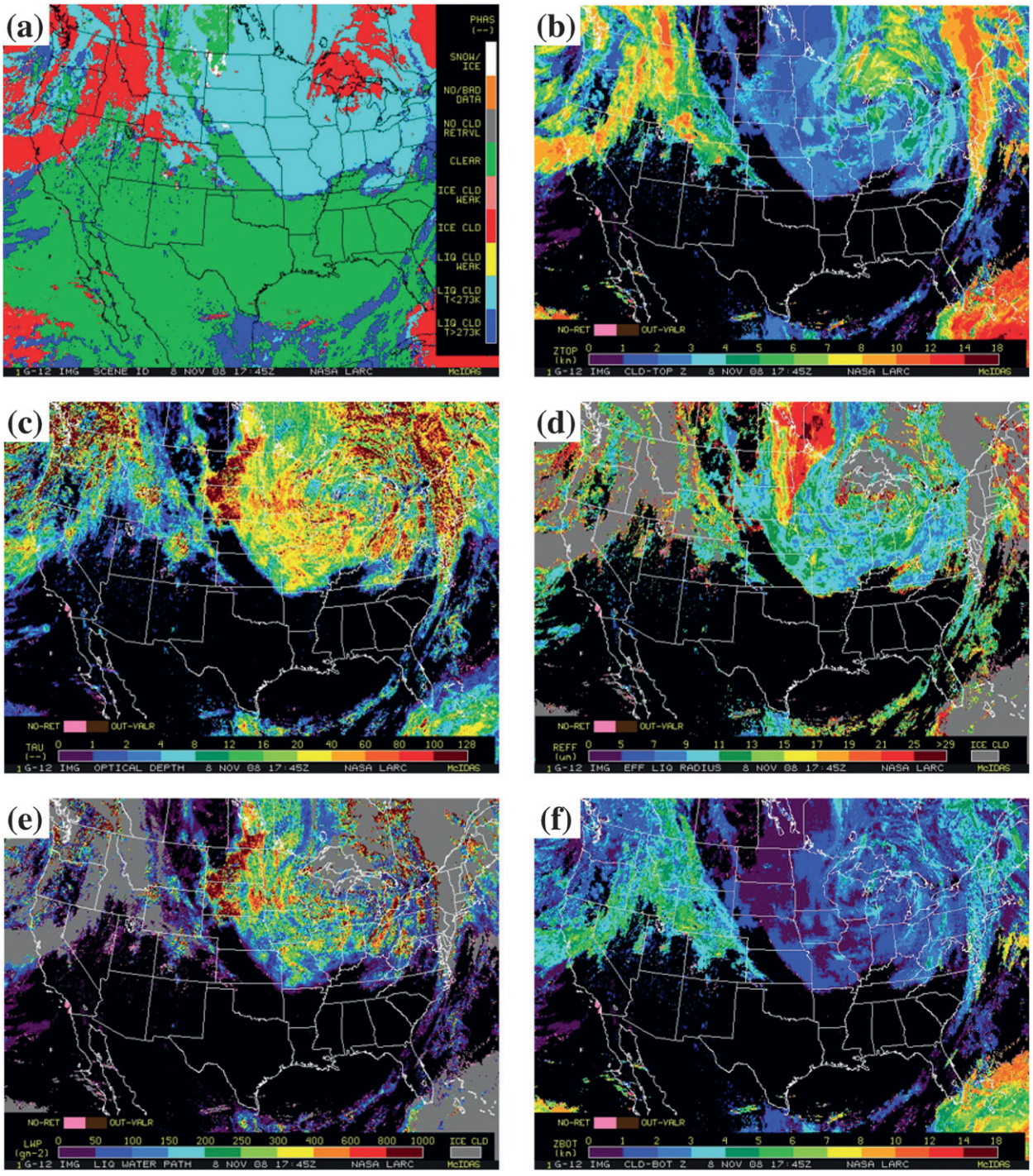

FIG. 1. Select cloud parameters derived from *GOES-E* and *GOES-W* at 1745 UTC 8 Nov 2008: (a) cloud-top phase, (b) cloud-top altitude (kft; 1 ft = 0.3048 m), (c) COD, (d) effective droplet size (μm) for liquid clouds, (e) LWP (g m^{-2}), and (f) base altitude (kft). These and other satellite-derived products are available online (http://angler.larc.nasa.gov).

interpret. A typical distribution of icing-intensity PIREPs shown in Fig. 2 for two winter periods over the CONUS indicates that most of the positive reports fall into only two of the eight possible intensity categories and that there are relatively few negative (''no icing'') reports. Icing PIREPs have been found to be useful for validating icing detection (Smith et al. 2000) but are inappropriate to compute standard measures of

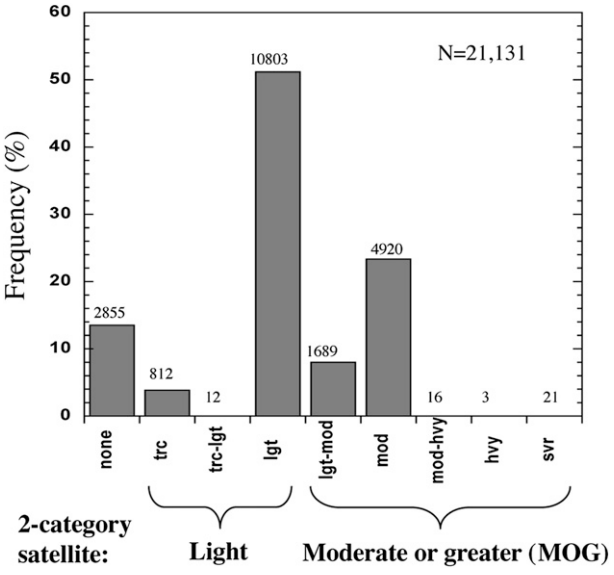

FIG. 2. PIREP icing intensity for two winter periods (November–March 2006/07 and 2007/08) over the CONUS. The classification strategy for the two-category satellite technique is also indicated.

overwarning, such as the false-alarm ratio (FAR; Brown and Young 2000).

c. TAMDAR

TAMDAR is the sensor currently deployed on approximately 400 commercial aircraft operating over the CONUS, Alaska, and Canada. TAMDAR is a low-cost sensor that was developed by AirDat, LLC, for NASA. It is designed to measure and report winds, temperature, humidity, turbulence, and icing from regional commercial aircraft (Daniels 2002). The TAMDAR icing sensor contains two independent infrared emitter–detector pairs mounted on the probe to detect ice accretion. The accretion of at least 0.5 mm of ice on the leading edge surface will block the beams and result in a positive detection. When ice is detected, internal heaters mounted within the probe melt the ice and the measurement cycle repeats. The heaters are powered for at least 1 min and the deicing cycle occurs each time ice is detected. The icing data are given as yes (icing) or no (no icing) reports. Thus, TAMDAR provides a direct, objective measure of the occurrence of in-cloud icing. Potential information on the icing intensity is not currently being extracted from the measurements. Data collected during the Great Lakes Fleet Experiment (GLFE) in 2005 are analyzed here to provide an initial assessment of their utility for validating the satellite FIT. The current TAMDAR deployment has shifted to include the western states and Alaska. These data will be analyzed in a future study.

d. NIRSS

The NIRSS has been collecting valuable information on icing conditions since 2005 at the NASA Glenn Research Center in Cleveland, Ohio. This location is well situated for observing icing conditions because it lies in the heart of a climatological icing bull's-eye (Bernstein et al. 2007). The NIRSS was developed to demonstrate a ground-based remote sensing system concept that could provide accurate detection and warning of in-flight icing conditions in the near-airport environment. The system fuses data from radar, lidar, and multifrequency microwave radiometer sensors to quantify the icing environment and compute the icing hazard (Reehorst et al. 2009) on the basis of the expected ice accretion severity for the measured environment (Politovitch 2003). Although the system does not measure icing directly, this remote sensing concept appears to offer some advantages for satellite validation that are not found elsewhere. For example, it appears that these unique data could help to quantify the FIT algorithm FAR, which cannot be done reliably with PIREPs or TAMDAR data. Several years of NIRSS data have been analyzed, and comparisons with the FIT derived from GOES are presented below.

3. Satellite methods

The potential for in-cloud aircraft icing and its severity depend on many factors related to the particular aircraft and the weather conditions. Some aircraft will accumulate ice in certain conditions while other aircraft will remain ice free in the same cloud. These aircraft-related factors are not considered here. Meteorological factors that contribute to icing intensity and severity include the concentration of supercooled water droplets and the droplet sizes. In general, larger droplets and/or larger concentrations of droplets or higher liquid water content (LWC) contribute to more severe icing. The satellite-derived R_e is related to the cloud droplet sizes while the derived LWP is related to the concentration since it is an estimate of the vertically integrated LWC. Correlations found between the satellite-derived LWP and R_e with icing PIREPs (Smith et al. 2003; Minnis et al. 2004) suggest that some information on icing intensity may be contained in the satellite data. The current version of the FIT algorithm has been developed 1) to exploit these relationships during the daytime for clouds that can be determined to pose an icing threat to aircraft because of the presence of SLW and 2) to take advantage of the capability to resolve highly variable cloud properties with high-resolution satellite data, as depicted in Fig. 1.

TABLE 1. Logic table for mapping the cloud phase and optical depth products to the icing mask.

Cloud phase	COD	Icing mask
Clear	—	No icing
Water	All	No icing
SLW	COD > 1.0	Icing
SLW	COD ≤ 1.0	No icing
Ice	COD ≤ 6.0	No icing
Ice	COD > 6.0	Unknown

a. Icing mask

Because SLW is a prerequisite for aircraft icing, the first step in the satellite FIT algorithm is to identify cloudy areas where SLW is likely to exist. An icing mask is constructed for each geolocated pixel with valid radiance data and for which the cloud algorithms have been properly executed and have returned valid retrievals. The purpose of the icing mask is to determine, to the extent possible, which cloudy pixels pose an icing threat to aircraft on the basis of the retrieved cloud-top temperature T_t, thermodynamic phase, and COD and to differentiate these pixels from clear and cloudy pixels that pose no icing threat or for which the icing threat cannot currently be determined (e.g., pixels composed of high-altitude optically thick ice-phase-topped clouds, or multilayered thin-ice-cloud-over-thick-liquid-cloud systems). The simple logic adopted to map the cloud-top phase and COD to the icing mask is shown in Table 1. A $T_t = 272$ K is used to distinguish warm water clouds from SLW clouds. For SLW clouds, a COD threshold of 1.0 is chosen to eliminate the very thinnest clouds associated with very low LWC values from the icing threat. For ice-phase-topped clouds, a COD threshold of 6.0 is used to eliminate thin clouds that are unlikely to overlap SLW clouds, while the icing threat for optically thicker clouds (COD > 6), which may or may not overlap SLW clouds, is considered to be unknown. The icing mask derived using the data from Fig. 1 is shown in Fig. 3 along with the icing intensity reported by pilots near the same time. Good correspondence is apparent between the icing PIREPs and the cyan areas representing potential icing conditions in the satellite-derived icing mask. Areas where there is no icing and where the icing threat cannot be determined are denoted by the gray and white colors, respectively.

b. Supercooled liquid water path

A potential issue in using an integral parameter such as the LWP as a proxy for icing in clouds with SLW tops is that it may include the mass of warm cloud water for clouds that extend to altitudes below the freezing level. A simple approach is adopted to estimate the supercooled fraction of the total LWP (SLWP) to eliminate the warm cloud mass from the icing threat. The approach requires knowledge of the cloud geometric thickness, the freezing level, and the vertical distribution of liquid water. The freezing level $Z_{\rm fr}$ is obtained from the satellite-derived T_t and Z_t, assuming a moist-adiabatic lapse rate:

$$Z_{\rm fr} = Z_t + (T_t - 273.15\,{\rm K})/6.5\,. \tag{1}$$

The cloud geometric thickness ΔZ is obtained using empirical formulas that depend on the COD (for water clouds) as described in Minnis et al. (2011a). For liquid water clouds,

$$\Delta Z = 0.39\ln({\rm COD}) - 0.01\,. \tag{2}$$

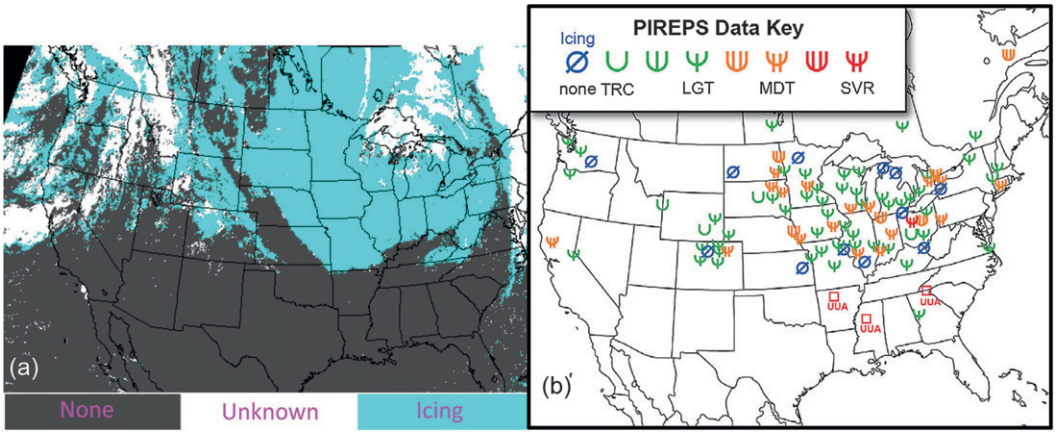

FIG. 3. (a) Icing mask at 1745 UTC and (b) corresponding pilot reports of icing intensity from 1600 to 2000 UTC 8 Nov 2008. The PIREP image was obtained online from the NOAA/National Weather Service (NWS) Aviation Weather Center (http://aviationweather.gov/adds/pireps/java/).

The minimum allowable ΔZ is 0.02 km. The cloud-base altitude Z_b is

$$Z_b = Z_t - \Delta Z. \quad (3)$$

For this study, a uniform vertical distribution of cloud liquid water is assumed. Thus, in this version, we define the SLWP as

$$\text{SLWP} = \text{LWP} \quad (Z_b \geq Z_{\text{fr}}) \quad \text{and} \quad (4)$$

$$\text{SLWP} = \text{LWP}(Z_t - Z_{\text{fr}})/\Delta Z \quad (Z_b < Z_{\text{fr}}). \quad (5)$$

c. Icing probability and intensity

Because of the nature of icing PIREPs and, in particular, of the fact that most positive icing-intensity reports fall into just two of the eight available intensity categories (light and moderate), a strategy is adopted to recategorize the eight intensity levels into two broader categories to serve as a more realistic target for the intensity component of the satellite algorithm. Hereinafter, ''light'' icing will be used to refer to reports in the first three PIREP intensity categories (trace, trace–light, and light), and ''moderate or greater'' (MOG) icing will refer to the other categories (light–moderate, moderate, moderate–heavy, heavy, and severe), as indicated in Fig. 2.

The icing PIREPs shown in Fig. 2 were matched with the coincident GDCP derived from *GOES-11* and *GOES-12* data taken over the CONUS to find relationships between icing and the satellite-derived cloud properties. Given the uncertainties in the PIREP locations, the satellite results were averaged in a 20-km-radius region centered at the location of each icing PIREP (about twenty-five 8-km pixels). This analysis was restricted to overcast SLW scenes as determined by the LaRC cloud-phase retrieval and to daytime [solar zenith angle (SZA) $< 82°$] data. Figure 4 depicts the frequency of occurrence of none, light, and MOG icing reports as a function of the GOES-derived SLWP. The results from the 1359 matches are binned in increments of 100 g m^{-2}. As SLWP increases, the number of negative and light icing reports decreases while the number of moderate or greater reports increases. Despite the aforementioned uncertainties associated with icing PIREPs and their superposition on high-resolution cloud fields such as the GOES-derived SLWP, which may be highly variable, the results in Fig. 4 are encouraging. Moreover, they are physically realistic considering that larger values of LWP are likely to be associated with larger values of LWC and/or larger cloud thickness. Thicker SLW clouds may be associated with an increased icing threat because of the likelihood that they increase the aircraft's exposure time to SLW as it passes through the cloud.

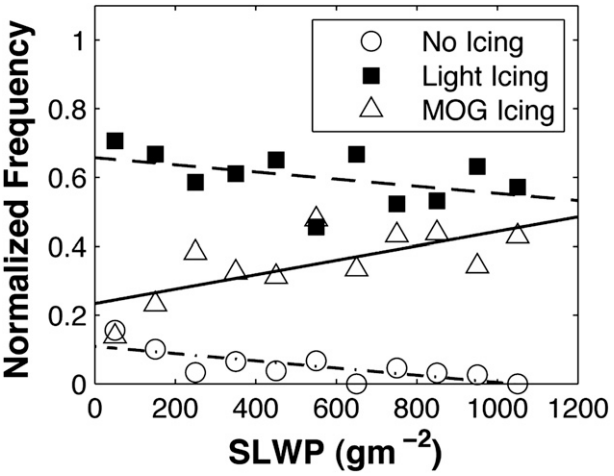

FIG. 4. Relative frequency of icing PIREPs vs GOES-derived SLWP for two winter periods (November–March 2006/07 and 2007/08) over the CONUS. The two-bin PIREP intensity categories are denoted as light and MOG, as in Fig. 2.

Using the data in Fig. 4, the probability of icing was computed as a function of SLWP. Those values were multiplied by the probability of icing found from the data for values of $R_e = 5$ μm (composed of data with $R_e < 8$ μm) and $R_e = 16$ μm (composed of data with $R_e \geq 16$ μm). These two sets of data were normalized to yield a 100% probability of icing for SLWP = 1050 g m^{-2} and $R_e = 16$ μm. These threshold values were chosen somewhat arbitrarily on the basis of visual interpretation of the data, since more definitive values could not be determined empirically. Thus, it is assumed that the combination of SLWP and R_e values at or above these thresholds yields a 100% probability for icing. The probabilities and best-fit curves for the two values of R_e, intended to represent the upper and lower limits, are shown in Fig. 5. In this procedure, the negative icing reports were duplicated several times to account for the sampling bias relative to positive icing reports that is apparent in Fig. 2. This bias in negative reports is due to the lack of incentive to report no icing. The results shown in Fig. 5 are consistent with our theoretical understanding of icing, indicating an increased likelihood of icing with increased SLWP and R_e. From these results, the icing probability (IP) is formulated in the FIT algorithm as

$$\text{IP} = 0.252 \log_{10}(\text{SLWP}) - 0.110 \quad (R_e = 5\,\mu\text{m}) \quad \text{and} \quad (6)$$

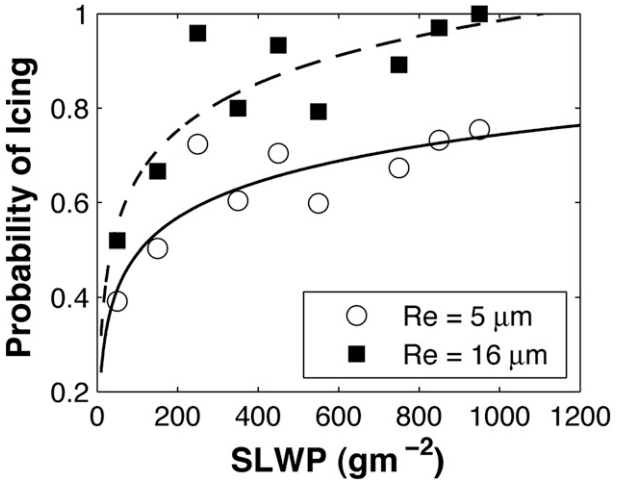

FIG. 5. Renormalized probability of in-cloud aircraft icing as a function of satellite-derived LWP and model fit for two values of R_e.

$$\mathrm{IP} = 0.333 \log_{10}(\mathrm{SLWP}) - 0.015 \quad (R_e = 16\,\mu\mathrm{m}). \qquad (7)$$

Linear interpolation between the results of (6) and (7) is used for pixels with R_e between 5 and 16 μm. Pixels with larger or smaller values of R_e are assigned the appropriate extreme value. Values of IP < 0.4 are classified as low probability. For values between 0.4 and 0.7, pixels are classified as medium probability, and values exceeding 0.7 are classified as high probability.

Table 2 lists the results of a statistical analysis performed on the matched satellite and icing PIREP dataset to determine any relationships between the GDCP and icing intensity. The mean and standard deviation for a number of satellite-derived cloud parameters are shown. When the values were computed with all of the matched data, the mean results indicate that, on average, there is little dependency found between icing-intensity PIREPs and R_e. There are several possible explanations for this result. In this analysis, R_e has been derived from the highly absorbing 3.9-μm channel, available on current GOES, which is mostly sensitive to cloud droplets very close to cloud top. It is possible that the cloud-top information extracted from this channel is not very representative of the droplet size spectra affecting icing conditions as reported by pilots, when the aircraft is well below cloud top. The scattering phase function for cloud hydrometeors is also very sensitive to droplet size when the solar angles and satellite viewing geometry are such that strong backscatter occurs, which may result in larger uncertainties or noise in the R_e retrievals. This phenomenon occurs in the late morning (early afternoon) for *GOES-E* (*GOES-W*) over the CONUS in the autumn and winter months when icing is most prevalent. More work is needed to reduce uncertainties in R_e retrievals using other satellites, multiple-wavelength R_e retrievals, and perhaps improved forward models to better understand and quantify any relationships between R_e and aircraft icing. A stronger dependence is found for the LWP, but there is not much separation between the mean LWP found for the light and MOG categories shown in the mean results when using all of the data.

To reduce the potential ambiguity associated with temporal and spatial matching errors on the correlations shown in the results for all data in Table 2, a strategy was adopted to filter the data. In the filtering procedure, a set of conservative SLWP thresholds is set for specific PIREP icing intensities on the basis of the assumption that the two are positively correlated as shown in Fig. 4. Thus, in the filtered dataset, the matched data are eliminated for the following scenarios: 1) all positive icing reports, if SLWP < 50 g m^{-2}; 2) all positive icing reports with MOG icing intensity, if SLWP $<$ 200 g m^{-2}; 3) all icing reports, if the intensity is less than light and the SLWP > 750 g m^{-2}; and 4) all icing reports with light or less intensity if SLWP > 1000 g m^{-2}. About 20% of the original matched data are absent in the filtered dataset. Much stronger sensitivity to LWP is found in the filtered dataset (Table 2) since the correlation

TABLE 2. Mean and standard deviation (in parentheses) found for satellite-derived cloud parameters matched with icing PIREPs during winters of 2006/07 and 2007/08 in three categories: 0 = no icing, 1 = light icing, and 2 = moderate or greater icing. Results are shown for the entire matched dataset (''all data'') and for the filtered dataset (''filtered data'').

Cloud property (GOES)	PIREP intensity (all data)			PIREP intensity (filtered data)		
	0	1	2	0	1	2
COD	35.98 (25.41)	42.89 (28.49)	49.60 (29.32)	31.25 (22.52)	35.74 (21.98)	56.71 (27.64)
R_e (μm)	11.65 (3.17)	12.03 (3.11)	12.11 (3.02)	11.35 (2.68)	12.00 (3.15)	12.11 (2.95)
LWP (g m^{-2})	460.56 (569.58)	614.21 (653.18)	715.54 (678.19)	321.61 (369.75)	381.67 (317.59)	836.65 (694.14)
SLWP (g m^{-2})	332.31 (444.03)	530.65 (592.64)	671.68 (664.48)	193.16 (160.45)	338.91 (232.74)	805.90 (676.69)
T_c (K)	263.39 (4.44)	262.65 (3.96)	262.05 (3.62)	263.62 (4.45)	262.61 (3.87)	261.84 (3.50)
ΔZ (km)	1.23 (0.36)	1.34 (0.37)	1.43 (0.36)	1.17 (0.33)	1.27 (0.29)	1.51 (0.34)
No.	90	838	431	79	659	346

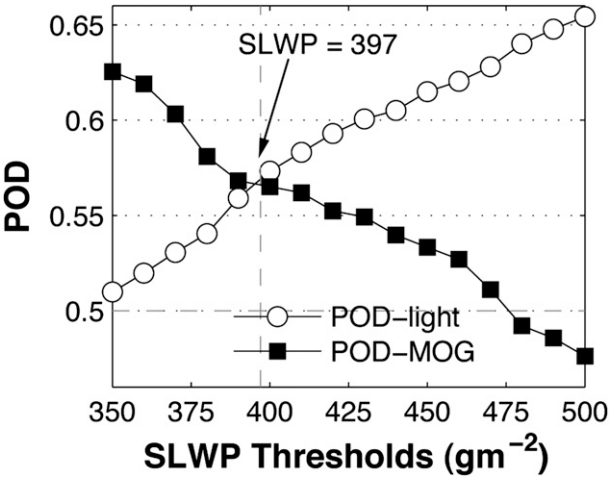

FIG. 6. Probabilities of detecting light and MOG icing conditions as a function of the GOES-derived SLWP in snow-free conditions during the winters of 2006/07 and 2007/08.

between the icing intensity and the LWP has increased. Also note that the filtered dataset generally produces much lower LWP standard deviations. From a statistical point of view, there is arguably good reason to employ the filtering procedure to both develop and validate the algorithm, but the procedure is somewhat arbitrary, and there is no guarantee or requirement that independent evaluators of the algorithm would also employ it. Thus, we have developed an approach to determine intensity thresholds for the current version of the FIT algorithm using all of the matched (unfiltered) data. We have, however, chosen to report the results that are shown in Table 2 to provide the mean cloud properties found for this icing dataset and to demonstrate the improved sensitivity of the LWP and SLWP to icing intensity reported by pilots when a simple filtering procedure is applied.

The filtering procedure is also employed in our validation studies (section 4) to help to bound the uncertainties. For the current algorithm, intensity thresholds were derived, using the unfiltered dataset, by iteratively determining the SLWP threshold that maximizes both the probability of detection for the light (PODL) and MOG (PODM) categories. Different thresholds were derived for snow and snow-free scenes since the snow albedo was not accounted for in this version of the LaRC cloud analyses. The bright snow background could bias the cloud microphysical property retrievals. An example for the snow-free dataset is shown in Fig. 6, which indicates a maximum POD of 0.55 for the two intensity categories at an SLWP threshold of 379 g m^{-2}. Daily snow maps obtained from the National Snow and Ice Data Center (now available from the National Ice Center: http://www.natice.noaa.gov) are used to stratify the matched satellite–PIREPs dataset for snow and snow-free scenes. Table 3 summarizes the SLWP thresholds and the intensity POD (PODL is equal to PODM in this technique) found following this approach for snow, snow-free, and all surfaces.

TABLE 3. The two-category intensity thresholds and probability of detection found using the satellite-derived SLWP over snow (100% coverage), snow-free (0% coverage), and all surfaces for consecutive winters (November–March) between 2006 and 2008.

Surface	SLWP (g m^{-2})	POD (%)	*N*
All	405	58	2341
Snow	475	63	735
No snow	379	55	1310

d. Algorithm output

The satellite-derived icing mask, probability, and intensity are combined to form the FIT index, depicted in Table 4, which is the primary output of the FIT algorithm. The FIT index is color coded for display purposes and is illustrated in Fig. 7 for the 8 November 2008 case. In general, there is good correspondence between the FIT output and the icing-intensity PIREPs shown in Fig. 3b. That is, warmer colors associated with more severe icing and the cooler colors associated with less severe or no icing tend to match reasonably well on a large scale. It is apparent how much more information the current FIT product can provide during the daytime when compared with a binary yes/no icing product (e.g., icing mask in Fig. 3). The approach described here may resolve some of the natural variability in the FIT to a significant degree but, of course, needs to be validated to the extent possible.

4. Verification

To help to gain an understanding of the potential utility of the satellite-based FIT product to the aviation

TABLE 4. FIT index output from the satellite FIT algorithm.

FIT index	Description
−7	No retrieval/bad data
−9	Missing data/other
0	No icing
1	Unknown
2	Low probability of light icing (daytime only: SZA < 82°)
3	Medium probability of light icing (daytime only: SZA < 82°)
4	High probability of light icing (daytime only: SZA < 82°)
5	High probability of MOG icing (daytime only: SZA < 82°)
6	Icing possible (Nighttime only: SZA ≥ 82°)

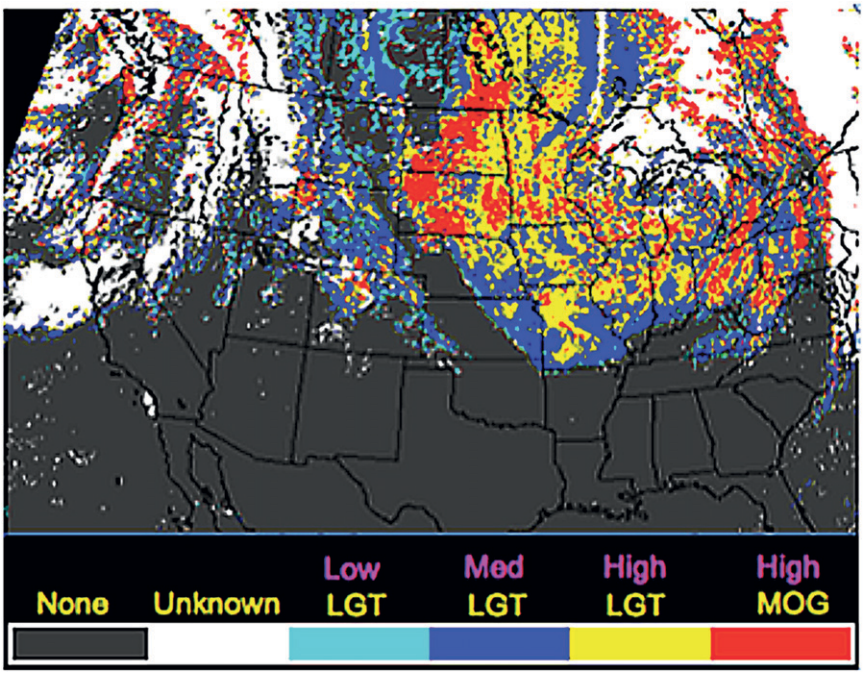

FIG. 7. Flight icing threat derived from GOES at 1745 UTC 8 Nov 2008.

community, icing information from PIREPs, TAMDAR, and NIRSS is used for intercomparison. Each dataset has unique advantages and disadvantages (described briefly in section 2), with their own associated uncertainties that may not be well understood in some cases. Because the satellite FIT algorithm has no vertical resolution and produces a bulk icing index limited to SLW-topped clouds (generally lower-level clouds with limited vertical extent that are not obscured by high-level clouds), and considering the uncertainties in satellite-derived boundary layer cloud heights and the uncertainties associated with the validation data, we have excluded altitude in our validation thus far. The matching approach that has been adopted here ensures to the extent possible that the satellite and validation data represent the same cloud volume. It is also important to emphasize again that aircraft icing is not just a meteorological phenomenon, but depends on characteristics of the airframe, flight trajectory, residence time, and other factors. Furthermore, there is currently no accepted definition for icing severity that is based on cloud microphysical parameters (e.g., LWC or R_e) or the accretion rate on an airframe (M. Politovitch, UCAR, 2010, personal communication).

Despite the somewhat ill-defined nature of aircraft icing, a method was developed to quantify the potential accuracy of the satellite product by correlating it with icing information extracted from PIREPs, TAMDAR, and NIRSS data. The data were matched in time and space for overcast conditions to eliminate any ambiguity that might arise in partly cloudy conditions. Two-by-two contingency tables are constructed to help to quantify the intercomparisons with standard skill scores (e.g., Wilks 2006). Each cell in the table provides the frequency with which a particular observation or estimate occurs at a specific threshold. Two sets of contingency tables are formed. The first table is composed of yes or no icing frequencies to test the icing-detection capability, as in Table 5. The second table is composed of light or MOG icing frequencies to test the icing-intensity capability, as in Table 6. The set of skill scores computed, and discussed below, is defined in Table 7.

a. Comparisons with icing PIREPs

The FIT derived from *GOES-11* and *GOES-12* was compared with icing PIREPs over the CONUS between

TABLE 5. Contingency table describing possible outcomes for icing detection.

	Icing observed	
Icing detected by satellite	Yes	No
Yes	*h* (hit)	*f* (false alarm)
No	*m* (miss)	*n* (correct negatives)

TABLE 6. As in Table 5, but for icing intensity.

Satellite intensity	Observed intensity	
	Light	MOG
Light	hL (light hit)	mM (MOG miss)
MOG	mL (light miss)	hM (MOG hit)

1 November and 31 March 2008–09 and 2009–10. This dataset is independent from that used in the algorithm development (2006–08). In this analysis, all pixels within 20 km and 15 min of each icing PIREP were matched under the condition that the 20-km-radius region was completely overcast. Regions containing any SLW are considered to be positive detections from GOES. This strategy resulted in 22 551 and 9851 matches during the daytime and nighttime, respectively. The skill in detecting icing conditions was determined from the contingency tables shown in Tables 8 and 9. The PODY, PODN, and accuracy are 62%, 42% and 61% (56%, 54%, and 56%), respectively, during daytime (nighttime). False detections are common, but compose only a small percentage of the total (FAR = 5%–6%). These results are nearly identical to those found by Ellrod and Bailey (2007) during wintertime. The large number of misses is due to the fact that this version of the satellite FIT algorithm, like that of Ellrod and Bailey (2007), cannot detect icing conditions below high-level ice clouds. When these ''undetectable'' conditions are eliminated from the validation dataset, the satellite FIT algorithm performance is much better. Tables 10 and 11 depict the contingency tables for the same data used to construct Tables 8 and 9 but excluding the cases with high optically thick ice cloud. Under these conditions, the PODY, PODN, and accuracy are found to be 98%, 6%, and 93% (64%, 49%, and 63%), respectively, during daytime (nighttime). It is not possible to adequately quantify false alarms using icing PIREPs because of the low bias in ''no icing'' observations (Brown and Young 2000). PODN is also highly uncertain and misleading for the same reason. The high values of PODY and accuracy found for the daytime data indicate that the satellite technique has an excellent detection capability relative to positive icing PIREPs, provided high clouds do not obscure the satellite view. The skill at night is good but is less than that found during the daytime because of the availability of just a few infrared channels that have poor sensitivity to optically thick cloud microphysical properties.

A contingency table was formed to test the two-category intensity component of the FIT algorithm during daytime for overcast SLW regions (number N = 5711) and is shown in Table 12. The probabilities of detecting light (PODL) and moderate or greater (PODM) icing conditions are 59% and 57%, respectively, and the accuracy is 58%. Considering the uncertainties associated with icing PIREPs and the associated difficulties in accurately matching the reports to satellite data, these comparison results are probably reasonable. The data were also stratified for snow and snow-free scenes. The intensity accuracy was also found to be 57% for both, which is an encouraging consistency indicating that the LWP thresholds developed with the 2006–08 data (Table 3) worked relatively well for the 2008–10 dataset. Better results were found using the filtering procedure described in section 3, which eliminates about 15% of, what appear to be, the more ambiguous data and yields a PODL, a PODM, and an intensity accuracy of 67%, 69%, and 67% respectively.

Figure 8 depicts a frequency histogram of cloud-top temperatures for all of the matched satellite and icing PIREP data used in this study between November 2006 and March 2010. The percentage of clouds with bases estimated to be below the freezing level is indicated for each 5-K temperature bin and is found to occur about 25% of the time, overall. To gauge the impact of our strategy to partition the cloud mass for the subfreezing portion (SLWP), the algorithm was also evaluated with data using intensity thresholds developed in the same manner described earlier but using the LWP rather than the SLWP. The overall improvement in the intensity accuracy using the SLWP approach is just a few percent

TABLE 7. Contingency-table scoring definitions.

Score	Meaning	Formula
PODY	Probability of detecting icing	$h/(h + m)$
PODN	Probability of detecting no icing	$n/(f + n)$
FAR	False-alarm ratio	$f/(h + f)$
Accuracy	Icing-detection accuracy	$(h + n)/(h + m + f + n)$
TSS	True skill score	PODY + (1 − PODN).
PODL	Probability of detecting light icing	hL/(hL + mL)
PODM	Probability of detecting MOG icing	hM/(hM +mM)
Intensity accuracy	Icing-intensity accuracy	(hL + hM)/(hL + mL + mM + hM)

TABLE 8. Frequency of yes/no icing reports found for the matched GOES–PIREP dataset constructed over consecutive winters (November–March) between 2008 and 2010 for overcast regions during daytime.

	Icing observed	
Icing detected by satellite	Yes	No
Yes	13 075	790
No	8107	579

TABLE 10. Frequency of yes/no icing reports found for the matched GOES–PIREP dataset constructed over consecutive winters (November–March) between 2008 and 2010 for overcast regions with no high thick clouds during daytime.

	Icing observed	
Icing detected by satellite	Yes	No
Yes	13 075	790
No	237	46

when evaluating all of the data. However, when considering only the data for which SLWP and LWP differ (occurs 25% of the time), a relative accuracy improvement of about 20% is realized using the SLWP approach.

b. Comparisons with NIRSS

The NIRSS icing retrieval uses ground-based remote sensing data to estimate the FIT over a single surface site (Reehorst et al. 2009) in Cleveland, Ohio. Although icing is not measured directly, NIRSS provides an objective estimate using active and passive remote sensors (i.e., microwave radiometer, cloud radar, and ceilometer) and thus has the capability to provide vertical resolution, with some assumptions. In the NIRSS approach, the vertical distribution of supercooled liquid water is estimated using climatological profiles that are based partially on experience and measurements taken from the NASA Glenn Twin Otter during icing research aircraft missions, and using the cloud radar reflectivity measured at the site. The profiles are constrained with the integrated liquid water (LWP) inferred from the microwave radiometer and cloud boundaries derived from the radar and ceilometer. For the subfreezing portion of the cloud, LWC is converted to eight levels of icing intensity with relationships that were developed from an airfoil modeling study (Politovitch 2003). An example of the NIRSS icing retrieval is shown in Fig. 9 along with the corresponding cloud boundaries and FIT derived from GOES on 12 February 2010. For this case, there is reasonably good agreement between the satellite-derived cloud boundaries and FIT with the NIRSS results.

Three years of NIRSS icing retrievals taken between 2008 and 2010 were analyzed and matched with the satellite data when the GDCP indicated overcast conditions. The icing threat was estimated from the GOES data using pixels within 20 km of the site. A bulk icing intensity was computed from the NIRSS results, for direct comparison with the satellite FIT, by averaging the vertical mean NIRSS LWC over a 20-min period centered at the time when *GOES-12* scanned Cleveland. The mean LWC was converted to icing intensity using the NIRSS conversion factors and the same categorical partitioning shown in Fig. 2. Contingency tables were constructed as before to evaluate the estimates of satellite icing detection and intensity relative to the NIRSS data. For this dataset, there were 885 matches, including 174 cases with high ice cloud obscuration. PODY, PODN, FAR and TSS were found to be 76%, 62%, 10%, and 38%, respectively. With respect to NIRSS data, the FIT-algorithm icing-detection accuracy is 73%. As before, eliminating the ''unknown'' cases yielded different statistics. In that case, the accuracy is 90%, and the PODY, PODN, FAR, and TSS are found to be 100%, 22%, 10%, and 22%, respectively. The low values of PODN and TSS are due to the relatively low number of no-icing cases (most of the NIRSS data were obtained during winter), and to a significant number of false alarms due to thin cirrus contamination in the satellite retrievals. A detailed analysis of the satellite and cloud radar imagery for the false-alarm points indicated that many of these cases were thin cirrus over warm water clouds, which were misclassified as SLW pixels in the satellite analyses.

The severity component of the FIT algorithm was also tested relative to the NIRSS data. The PODL and PODM were found to be remarkably consistent, with values of 77% and 78%, respectively. The overall accuracy in the FIT intensity is 77%. These results are

TABLE 9. As in Table 8, but during nighttime.

	Icing observed	
Icing detected by satellite	Yes	No
Yes	5158	273
No	4104	316

TABLE 11. As in Table 10, but during nighttime.

	Icing observed	
Icing detected by satellite	Yes	No
Yes	5158	273
No	2859	261

TABLE 12. Frequency of the two-category icing intensity found for the matched GOES–PIREP dataset constructed over consecutive winters (November–March) between 2008 and 2010 for regions determined from GOES to contain overcast SLW clouds.

	Observed intensity	
Satellite intensity	Light	MOG
Light	2385	716
MOG	1675	935

encouraging considering that the FIT algorithm is tuned to icing PIREPs while the NIRSS intensity is tuned to an airfoil model, and considering the different sensitivities and assumptions associated with the satellite and ground-based remote sensing techniques.

c. Comparisons with TAMDAR

The FIT algorithm was applied to the GDCP derived from daytime *GOES-12* data from 1 to 26 April 2005 and was compared with TAMDAR data taken during the GLFE. The pixel-level icing parameters derived from GOES are averaged, by spatially weighting the four closest pixels to each TAMDAR observation taken within 15 min of the satellite observation. There were 440 542 TAMDAR observations, of which 13 321 indicated icing, 8951 indicated that the heater was on so that icing was not detectable at that time, and the rest indicated that no icing was observed. Unlike the relatively few PIREPs (most of which are reported during icing conditions), TAMDAR takes continuous data. As a result, about 95% of the TAMDAR reports indicate no icing. Thus, the GOES and TAMDAR comparison statistics in the results will be biased toward the TAMDAR no-icing category if filters are not properly applied to remove insignificant reports (e.g., from cloud-free areas).

Figure 10 shows an example of satellite-derived icing indices compared with the TAMDAR icing indicators on a Mesaba Airlines flight (with TAMDAR serial number 247) between 1800 and 1830 UTC 22 April 2005. Good agreement is found for this single-layer cloud case. The satellite FIT is a bulk index for the icing layer as indicated by the vertical bars. The TAMDAR measurements indicating yes or no icing are also plotted as a function of altitude. During the majority of the flight segment, the aircraft was inside the GOES-retrieved cloud boundaries and reported icing that corresponds well to the GOES analysis. During the descent below cloud base, the TAMDAR no longer reported icing while GOES still detected icing above the aircraft. This illustrates the need to ensure, to the extent possible, that only in-cloud TAMDAR reports be compared with the GOES FIT.

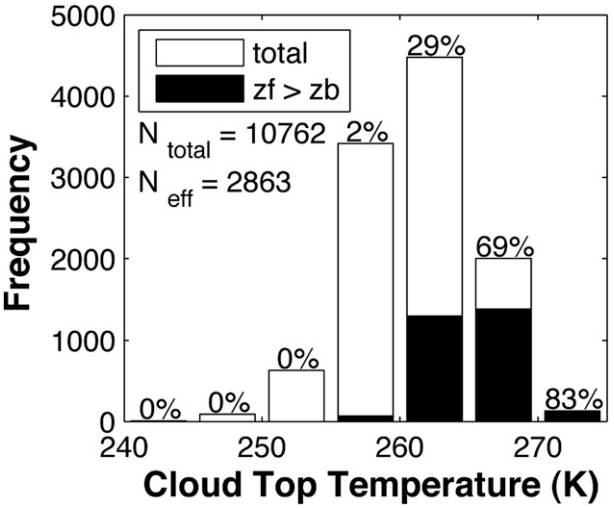

FIG. 8. Frequency histogram of cloud-top temperature for all of the matched satellite and icing PIREP data used in this study between November 2006 and March 2010. The percentage of clouds with bases estimated to be below the freezing level is indicated for each 5-K temperature bin.

To compare statistically the TAMDAR data with GOES without biasing the results, only TAMDAR reports at altitudes within the GOES-derived cloud boundaries are used. This condition reduced the total number of daytime TAMDAR reports (with heater off) to 17 140. This includes 5048 cases in which icing could not be determined from GOES because of obscuration by high ice clouds. If we classify these points as no icing from GOES, then the PODY, PODN, accuracy, and FAR are found to be 45%, 67%, 72%, and 85%, respectively. Eliminating the GOES unknown points yields values of 87%, 49%, 53%, and 85%. Thus, a reasonable value for PODY (87%) was found using TAMDAR, which agrees well with the values found with the other validation datasets, but the remaining statistics are relatively poor. This is due to the high number of false alarms (FAR is 84%), most of which were determined to arise as a result of inaccuracies in the cloud altitude boundaries derived from GOES. Because the retrieved cloud-base and -top heights have an uncertainty of about 1 km (Smith et al. 2008), it is likely that many of the TAMDAR no-icing reports outside of clouds are being included in the statistics with the GOES icing detections. Thus, the PODY appears to be the only derived metric with much value, considering the comparison method used here. We plan to use the temperature and humidity profiles in future analyses of TAMDAR data to try to improve the definition of the actual cloud boundaries penetrated by the instrumented aircraft and, it is

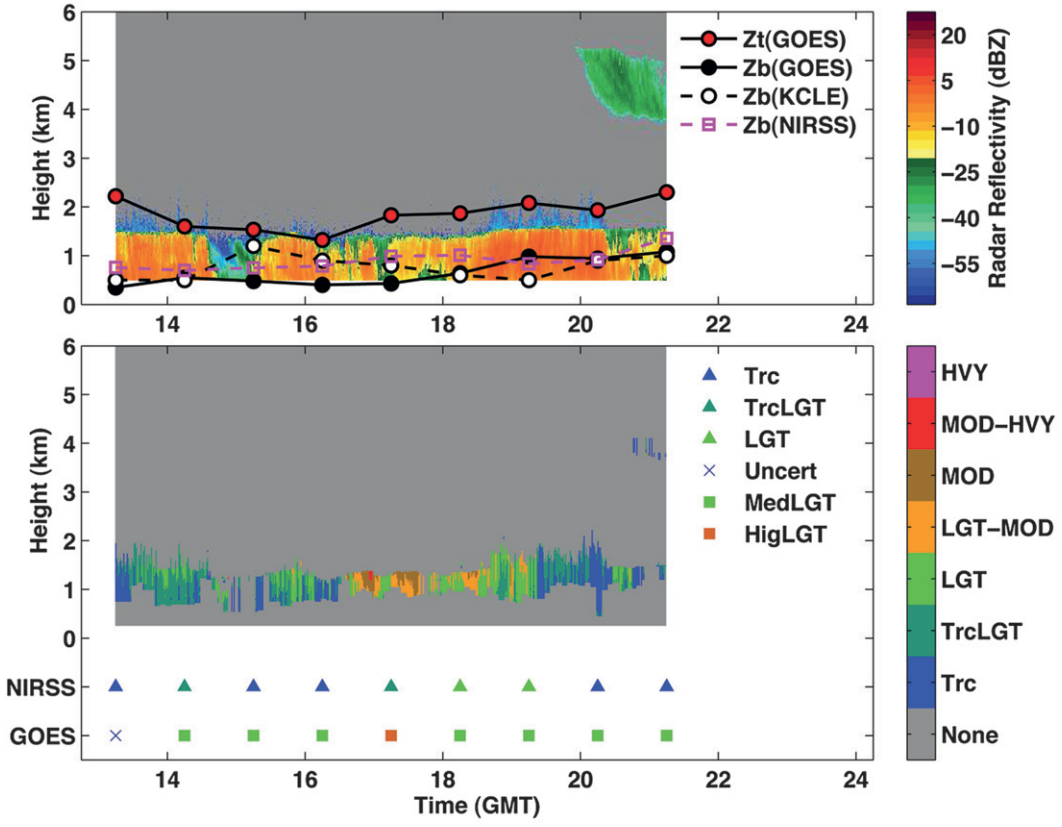

FIG. 9. Comparison of flight icing threats derived from NIRSS and GOES for 12 Feb 2010. (top) NIRSS radar reflectivity and (bottom) icing-intensity profiles with satellite-derived cloud boundary overlay (red and black circles). Cloud base measured by ceilometer is shown for the NIRSS site (pink squares) and at a nearby NWS Automated Surface Observing System station (white circles). Vertical and temporal aggregate NIRSS icing is indicated by colored triangles at the bottom of the bottom panel along with the FIT derived from GOES, which is indicated by the colored squares.

hoped, to improve the utility of TAMDAR data for satellite validation.

5. Summary

In this paper, a physically based empirical technique was developed to estimate from satellite data the FIT to aircraft. The technique is formulated to utilize satellite-derived cloud products as input, including T_c, cloud-top phase, LWP, and R_e. The satellite-based icing method has been applied to current GOES data, and the results were rigorously compared with icing observations contained in PIREP, TAMDAR, and NIRSS data. A summary of these comparisons is provided in Table 13. During the daytime, the satellite icing detection accuracies are found to range from about 60% to 75% using the various validation sets as ground truth in all cloud conditions. The results that are based on comparisons with icing PIREPs are nearly identical to those found by Ellrod and Bailey (2007), who used a radiance thresholding technique. Much better results are obtained if we use the satellite-derived cloud microphysical properties to screen out the cases obscured by high ice clouds, since the presence of SLW below these clouds cannot be inferred with current single-layer satellite retrieval methods. Excluding these cases yields accuracies of 90% or better when compared with NIRSS and PIREPs. The poor accuracy found in the comparisons with TAMDAR can be attributed to insufficient knowledge of when the TAMDAR sensor is reporting no-icing conditions in cloud rather than in clear air. From the data shown in Tables 8–11, we estimate that roughly 35% of atmospheric icing remains undetected using single-layer techniques, because of high cloud obscuration. New techniques (e.g., Chang et al. 2010) to derive cloud properties in some multilayer conditions [i.e., thin cirrus over lower-level water clouds; see Chang and Li (2005)] can be exploited to estimate the FIT below high-level ice clouds with a promising degree of accuracy. This is a topic for future research that may

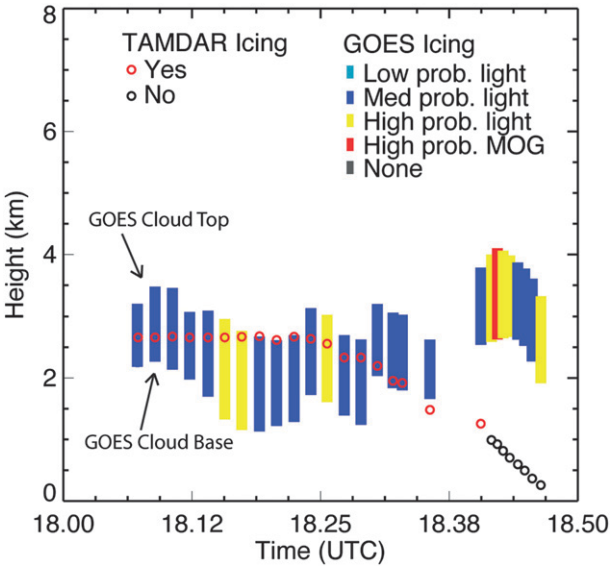

FIG. 10. Comparison of the GOES-derived flight icing threat to yes/no icing inferred using TAMDAR sensor measurements taken from a commercial aircraft on 22 Apr 2005 during the GLFE.

further improve the satellite-derived FIT under a wider range of cloud conditions.

A significant advance in the FIT algorithm developed here, relative to previous satellite-based icing analyses, is an estimate of icing probability and intensity that is based on derived cloud microphysical parameters. The technique significantly increases the information content extracted from the satellite observations, providing an improved dynamic range to the FIT that should be useful to the aviation community. Relative to icing PIREPs, the accuracy in the satellite two-category intensity estimates is between 58% and 68% depending on the degree of filtering used to reduce ambiguities that are likely due to poor spatial and temporal matching. Better agreement is found with NIRSS data (77% accuracy), which is also encouraging, keeping in mind that NIRSS is a ground-based remote sensing system and does not provide a direct measure of icing intensity. The results presented here indicate that the satellite method has significant skill. Considering the somewhat ill-defined nature of icing intensity and severity, as well as many issues regarding the accuracy of the validation data used to characterize aircraft icing, it is possible that the practical utility of the method to the aviation community may be better than the validation data suggest, but this remains to be demonstrated.

Newer advanced imagers, with more channels and improved horizontal resolution and spectral information similar to that currently available on MODIS, such as the Visible Imaging Infrared Radiometer Suite on the Suomi National Polar-Orbiting Partnership, the Spinning Enhanced Visible and Infrared Imager (SEVIRI) on the Meteosat series deployed over Europe, and the Advanced Baseline Imager planned for GOES-R, are providing the impetus for research to further advance satellite-derived cloud characterizations for icing and other aviation weather hazards. For example, advanced imagers can provide some capability to improve the resolution of cloud vertical structure (e.g., Platnick 2000), which has not yet been exploited. It is also expected that the icing-detection accuracy at night and during the day/night transition will be somewhat better than that shown in Table 13 because of the availability of additional spectral information in the infrared with improved sensitivity to cloud-top phase (Pavolonis 2010). Despite the inherent bias toward ''positive icing'' reports found in the validation data used in this study, we were able to gain some understanding of potential false alarms, which appear to occur less than 10% of the time. A significant number of these cases appear to be due to the inability to detect thin cirrus clouds adequately with the current GOES imager in multilayer conditions. Improvements can be expected in the near future that take advantage of the improved resolution and spectral information available from advanced imagers, as well as improved cloud retrieval techniques, including the multilayer methods currently being developed.

TABLE 13. Summary of the FIT capability determined from GOES when compared with icing PIREP, TAMDAR, and NIRSS data for all cloud conditions, and under the condition that high-level overcast ice clouds do not obscure the satellite view. The intensity accuracy was only evaluated in overcast SLW conditions as determined from GOES.

		Icing detection				
		All clouds		Unobscured		
Validation data	Day/night	PODY (%)	Accuracy (%)	PODY (%)	Accuracy (%)	Icing-intensity accuracy (%)
PIREPs	Night	56	56	64	63	—
PIREPs	Day (all)	62	61	98	93	58
PIREPs	Day (filtered)	—	—	—	—	67
NIRSS	Day	76	73	100	90	77
TAMDAR	Day	45	72	87	53	—

The satellite-based icing product described here, as well as the icing altitude boundaries derived from Z_t, Z_b, and Z_{fr}, provide unique information about icing conditions over broad areas and at resolutions not available elsewhere that should contribute a substantial enhancement in aviation safety to regions susceptible to heavy supercooled liquid water clouds. These icing products, as well as many other cloud and radiation products being derived routinely from operational satellite data, are available in digital and graphical formats from NASA (http://angler.larc.nasa.gov).

Acknowledgments. This research was supported by the NASA Applied Sciences Program and by the NOAA GOES-R program. We thank David Serke of NCAR-RAL and Andrew Reehorst of NASA Glenn Research Center for providing the NIRSS data and for useful discussions regarding its use. We also thank the three anonymous reviewers for their valuable comments and suggestions. The views, opinions, and findings contained in this report are those of the author(s) and should not be construed as an official NASA or U.S. government position, policy, or decision.

REFERENCES

Bernstein, B. C., F. McDonough, M. Politovich, B. Brown, T. Ratvasky, D. Miller, C. Wolff, and G. Cunning, 2005: Current icing potential: Algorithm description and comparison with aircraft observations. *J. Appl. Meteor.,* **44,** 969–986.

——, C. A. Wolff, and P. Minnis, 2006: Practical application of NASA-Langley advanced satellite products to in-flight icing nowcasts. *Proc. 44th AIAA Aerospace Science Meeting and Exhibit,* Reno, NV, AIAA-2006-1220.

——, ——, and F. McDonough, 2007: An inferred climatology of icing conditions aloft, including supercooled large drops. Part I: Canada and the continental United States. *J. Appl. Meteor. Climatol.,* **46,** 1857–1878.

Brown, B. G., and G. S. Young, 2000: Verification of icing and turbulence forecasts: Why some verification statistics can't be computed using PIREPs. Preprints, *Ninth Conf. on Aviation, Range, and Aerospace Meteorology,* Orlando, FL, Amer. Meteor. Soc., 393–398.

Chang, F.-L., and Z. Li, 2005: A new method for detection of cirrus overlapping water clouds and determination of their optical properties. *J. Atmos. Sci.,* **62,** 3993–4009.

——, P. Minnis, B. Lin, M. M. Khaiyer, R. Palikonda, and D. A. Spangenberg, 2010: A modified method for inferring upper troposphere cloud top height using the *GOES 12* imager 10.7 and 13.3 μm data. *J. Geophys. Res.,* **115,** D06208, doi:10.1029/2009JD012304.

Curry, J. A., and G. Liu, 1992: Assessment of aircraft icing potential using satellite data. *J. Appl. Meteor.,* **31,** 605–621.

Daniels, T. S., 2002: Tropospheric airborne meteorological data reporting (TAMDAR) sensor development. *SAE General Aviation Technology Conf. and Exposition,* Wichita, KS, SAE International, 2002-02-153. [Available online at http://papers.sae.org/2002-01-1523.]

Dong, X., P. Minnis, G. G. Mace, W. L. Smith Jr., M. Poellot, R. T. Marchand, and A. D. Rapp, 2002: Comparison of stratus cloud properties deduced from surface, GOES, and aircraft data during the March 2000 ARM Cloud IOP. *J. Atmos. Sci.,* **59,** 3256–3284.

——, ——, B. Xi, S. Sun-Mack, and Y. Chen, 2008: Comparison of CERES-MODIS stratus cloud properties with ground-based measurements at the DOE ARM Southern Great Plains site. *J. Geophys. Res.,* **113,** D03204, doi:10.1029/2007JD008438.

Ellrod, G., and J. P. Nelson, 1996: Remote sensing of aircraft icing regions using GOES multispectral imager data. Preprints, *15th Conf. on Weather Analysis and Forecasting,* Norfolk, VA, Amer. Meteor. Soc., 9–12.

——, and A. P. Bailey, 2007: Assessment of aircraft icing potential and maximum icing altitude from geostationary meteorological satellite data. *Wea. Forecasting,* **22,** 160–174.

Haggerty, J., F. McDonough, J. Black, S. Landolt, C. Wolff, S. Mueller, P. Minnis, and W. L. Smith Jr., 2008: Integration of satellite-derived cloud phase, cloud-top height, and liquid water path into an operational aircraft icing nowcasting system. Preprints, *13th Conf. on Aviation, Range, and Aerospace Meteorology,* New Orleans, LA, Amer. Meteor. Soc., 3.13. [Available online at http://ams.confex.com/ams/pdfpapers/131893.pdf.]

Kane, T. L., B. G. Brown, and R. Bruintjes, 1998: Characteristics of pilot reports of icing. Preprints, *14th Conf. on Probability and Statistics,* Phoenix, AZ, Amer. Meteor. Soc., 90–95.

Mason, J. G., J. W. Strapp, and P. Chow, 2006: The ice particle threat to engines in flight. *Proc. 44th AIAA Aerospace Science Meeting and Exhibit,* Reno, NV, AIAA-2006-206.

Minnis, P., and Coauthors, 1995: Cloud Optical Property Retrieval (subsystem 4.3). Clouds and the Earth's Radiant Energy System (CERES) Algorithm Theoretical Basis Document: Cloud Analyses and Radiance Inversions (Subsystem 4), NASA RP 1376, Vol. 3, 135–176.

——, and Coauthors, 2004: Real-time cloud, radiation, and aircraft icing parameters from GOES over the USA. Preprints, *13th Conf. on Satellite Oceanography and Meteorolology,* Norfolk, VA, Amer. Meteor. Soc., P7.1. [Available online at http://ams.confex.com/ams/pdfpapers/79179.pdf.]

——, and Coauthors, 2008a: Near-real time cloud retrievals from operational and research meteorological satellites. *Remote Sensing of Clouds and the Atmosphere XIII,* R. H. Picard et al., Eds., International Society for Optical Engineering (SPIE Proceedings Vol. 7107), 710703, doi:10.1117/12.800344.

——, and Coauthors, 2008b: Cloud detection in non-polar regions for CERES using TRMM VIRS and *Terra* and *Aqua* MODIS data. *IEEE Trans. Geosci. Remote Sens.,* **46,** 3857–3884.

——, C. R. Yost, S. Sun-Mack, and Y. Chen, 2008c: Estimating the physical top altitude of optically thick ice clouds from thermal infrared satellite observations using *CALIPSO* data. *Geophys. Res. Lett.,* **35,** L12801, doi:10.1029/2008GL033947.

——, and Coauthors, 2011a: CERES edition-2 cloud property retrievals using TRMM VIRS and *Terra* and *Aqua* MODIS data, Part I: Algorithms. *IEEE Trans. Geosci. Remote Sens.,* **49,** 4374–4400.

——, and Coauthors, 2011b: CERES edition-2 cloud property retrievals using TRMM VIRS and *Terra* and *Aqua* MODIS data, Part II: Examples of average results and comparisons with other data. *IEEE Trans. Geosci. Remote Sens.,* **49,** 4401–4430.

National Aviation Safety Data Analysis Center, 2005: National Transportation Safety Board weather related accident study: 1994–2003. Federal Aviation Administration Study Rep. [Available online at http://www.asias.faa.gov/aviation_studies/weather_study/studyindex.html.]

Pavolonis, M. J., 2010: Advances in extracting cloud composition information from spaceborne infrared radiances—A robust alternative to brightness temperatures. Part I: Theory. *J. Appl. Meteor. Climatol.,* **49,** 1992–2012.

Platnick, S., 2000: Vertical photon transport in cloud remote sensing problems. *J. Geophys. Res.,* **105,** 22 919–22 935.

Politovich, M. K., 2003: Predicting inflight aircraft icing intensity. *J. Aircr.,* **40,** 639–644.

Rasmussen, R., and Coauthors, 1992: Winter Icing and Storms Project (WISP). *Bull. Amer. Meteor. Soc.,* **73,** 951–974.

Rauber, R., and A. Tokay, 1991: An explanation for the existence of supercooled water at the top of cold clouds. *J. Atmos. Sci.,* **48,** 1005–1023.

Reehorst, A., D. Brinker, M. Politovich, D. Serke, C. Ryerson, A. Pazmany, and F. Solheim, 2009: Progress towards the remote sensing of aircraft icing hazards. NASA Tech. Rep. NASA/TM-2009-215828, 12 pp. [Available online at http://icebox-esn.grc.nasa.gov/RSData/70880J.pdf.]

Smith, W. L., Jr., P. Minnis, and D. F. Young, 2000: An icing product derived from operational satellite data. Preprints, *Ninth Conf. on Aviation, Range, and Aerospace Meteorology,* Orlando, FL, Amer. Meteor. Soc., 256–259.

——, ——, B. C. Bernstein, F. McDonough, and M. M. Khaiyer, 2003: Comparison of super-cooled liquid water cloud properties derived from satellite and aircraft measurements. *Proc. In-Flight Icing/De-icing Int. Conf.,* Chicago, IL, Federal Aviation Administration 2003-01-2156.

——, ——, H. Finney, R. Palikonda, and M. M. Khaiyer, 2008: An evaluation of operational GOES derived single-layer cloud top heights with ARSCL over the ARM Southern Great Plains site. *Geophys. Res. Lett.,* **35,** L13820, doi:10.1029/2008GL034275.

Thompson, G., R. Bullock, and T. F. Lee, 1997: Using satellite data to reduce spatial extent of diagnosed icing. *Wea. Forecasting,* **12,** 185–190.

Wilks, D. S., 2006: *Statistical Methods in the Atmospheric Sciences*. Academic Press, 627 pp.

Xi, B., X. Dong, P. Minnis, and M. M. Khaiyer, 2010: A 10-year climatology of cloud cover and vertical distribution derived from both surface and GOES observations over the DOE ARM SGP site. *J. Geophys. Res.,* **115,** D12124, doi:10.1029/2009JD012800.